

This is an Open Access document downloaded from ORCA, Cardiff University's institutional repository: <https://orca.cardiff.ac.uk/id/eprint/93683/>

This is the author's version of a work that was submitted to / accepted for publication.

Citation for final published version:

Kellici, Suela, Acord, John, Vaughn, Arni, Power, Nicholas P., Morgan, David John, Heil, Tobias, Facq, Sébastien P. and Lampronti, Giulio I. 2016. Calixarene assisted rapid synthesis of silver-graphene nanocomposites with enhanced antibacterial activity. *ACS Applied Materials & Interfaces* 8 (29), pp. 19038-19046. 10.1021/acsami.6b06052

Publishers page: <http://dx.doi.org/10.1021/acsami.6b06052>

Please note:

Changes made as a result of publishing processes such as copy-editing, formatting and page numbers may not be reflected in this version. For the definitive version of this publication, please refer to the published source. You are advised to consult the publisher's version if you wish to cite this paper.

This version is being made available in accordance with publisher policies. See <http://orca.cf.ac.uk/policies.html> for usage policies. Copyright and moral rights for publications made available in ORCA are retained by the copyright holders.



Calixarene Assisted Rapid Synthesis of Silver-Graphene Nanocomposites with Enhanced Antibacterial Activity

Suela Kellici,^{a} John Acord,^b Nicholas P. Power,^b Arni Vaughn,^a, David J. Morgan,^c Tobias Heil,^d Sébastien P. Facq,^e Giulio I. Lampronti^e and Simon Redfern^e*

^aSchool of Engineering, London South Bank University, 103 Borough Road, London, SE1 0AA, UK. *E-mail: kellicis@lsbu.ac.uk

^bSchool of Applied Sciences, London South Bank University, 103 Borough Road, London, SE1 0AA, UK.

^cCardiff Catalysis Institute, School of Chemistry, Cardiff University, Park Place, Cardiff, CF10 3AT, UK.

^dNanoinvestigation Centre at Liverpool, 1-3 Brownlow Street, Liverpool University, Liverpool, L69 3GL, UK.

^eDepartment of Earth Sciences, University of Cambridge, Downing Street, Cambridge, CB2 3EQ, UK.

KEYWORDS: graphene, silver, nanocomposite, antibacterial, calixarene, hydrothermal

ABSTRACT: Demonstrated herein is a single rapid approach employed for synthesis of Ag-graphene nanocomposites, with excellent antibacterial properties and low cytotoxicity, by utilizing a Continuous Hydrothermal Flow Synthesis (CHFS) process in combination with *p*-hexasulfonic acid calix[6]arene (SCX6) as an effective particle stabilizer. The nanocomposites showed high activity against *E. coli* (Gram-negative) and *S. aureus* (Gram-positive) bacteria. The Ag-graphene nanocomposites were characterized using a range of techniques including transmission electron microscopy (TEM), X-ray photoelectron spectroscopy (XPS), Raman, UV-Vis spectrophotometry and X-ray powder diffraction (XRD). This rapid, single step synthetic approach not only provides a facile means of enabling and controlling graphene reduction (under alkaline conditions), but also offers an optimal route for homogeneously producing and depositing highly crystalline Ag nanostructures into reduced graphene oxide substrate.

INTRODUCTION

Due to the growing concern for increasing antibacterial resistance by a number of different pathogenic bacteria and the associated threat to global public health, there is an imperative for researchers to not only find new antibiotic drugs, but to look at new avenues and or materials for use as antimicrobial agents to manage the problem.¹ Current materials are proving inadequate with performance/cost limitations a consequence of either increased antibacterial resistance, chemical instability, or short product life expectancy.² This gives an impetus for development of new materials, using low cost, efficient, and rapid manufacturing production routes.

The emerging class of 2-dimensional (2D) nanomaterials have attracted tremendous interest from both academia and industry due to their wealth of remarkable properties occurring as a result

of their atomic thickness and infinite lateral dimensions. Graphene is a single atomic thick sheet of sp^2 bonded carbon atoms most commonly derived from the exfoliation of graphite. The graphene oxide (GO) formed from the chemical exfoliation of graphite contains oxygenated functional groups such as epoxide groups on the surface of its basal plane and carboxylic groups at the edges.³ Removing these functional groups by chemical or thermal treatments produces reduced graphene oxide (rGO).⁴ However, although these materials have demonstrated some very interesting applications, including antibacterial activity^{3,4} with minimal cytotoxicity to animal and human cells,⁵ as standalone material it does not possess the diversity of properties that are required to allow integration in to a range of potential technological applications including as antimicrobial agents.

The use of nanoscale inorganic materials, such as zinc oxide³, titanium dioxide⁶, and gold⁷, have been found to have antimicrobial properties due to a number of their unique physical and chemical properties, such as their high surface to volume ratio.⁸ However, both historically and more recently, silver nanoparticles (Ag) have been shown to display some of the most efficient bactericidal properties.⁸ For example the antimicrobial mechanisms performed by Ag nanoparticles have been demonstrated through their interaction with thiol groups of cell membrane proteins and phosphorus groups of cytoplasm, negatively affecting the functions of cellular respiration and division, eventuating in cell death.⁸ Silver's exceptional optical, electronic, and catalytic properties at the nanoscale, has seen it utilized in a wide range of applications from solar cells to optical sensors for biomolecule detection.⁹

A drawback to using Ag nanoparticles is their affinity to form aggregates resulting in decreased stability,¹⁰ which in turn reduces their antibacterial effectiveness.⁸ This can be overcome by depositing Ag nanoparticles onto a support material such as 2D-rGO nanosheets.⁸ These Ag-

graphene hybrids have large surface areas and strong van der Waals forces between the two materials, where the problem of agglomeration of Ag is reduced whilst stability of the nanoparticles is increased.¹¹ Similarly, rGO, due to its negatively charged surface, has an enhanced adsorption ability which should allow it to adsorb bacterium onto its surface, resulting in greater contact of the deposited Ag nanoparticles with the bacterial cells.⁸ It has been reported that using Ag-rGO nanocomposites as a bactericidal could produce equivalent effectiveness compared to the common antibacterial drug ampicillin.⁸ We herein report the synthesis of an Ag-calixarene-rGO hybrid material that can possibly outperform commercial antibiotics such as ampicillin. Therefore, by combining the properties of both nanomaterials we can increase stability, reduce agglomeration and maintain effectiveness, whilst developing a low cost, efficient, and scalable manufacturing procedure.

Generally the production of Ag nanoparticles involves the reduction of silver salts (Ag^+) by strong reductants such as hydrazine (N_2H_4) or, from the Creighton method, sodium borohydride (NaBH_4), or by hydrogen gas which carry the burden of toxicity or pressurized gas systems.^{9, 10} Therefore an approach to synthesize the desired materials and limiting the potential risk to human health and to the environment is needed. These challenges can be answered by the production of Ag nanoparticles for antibacterial applications, *via* a Continuous Hydrothermal Flow Synthesis (CHFS) approach, which offers an attractive solution that affords a more tailored and advanced development of functional 2D materials with minimal structural and electronic defects.

CHFS, a single step process, involves mixing (in a bespoke mixer/reactor) a flow of superheated water to its critical point or higher (374 °C, 22.1 MPa) with a flow of water-soluble precursor(s) (often metal salts) to give rapid synthesis (within seconds) and controlled growth of nanomaterials in a continuous manner. CHFS approaches are unique and represent significant advantages in

materials synthesis; it utilizes a continuous flow procedure reducing complexity and timescale, and offers a positive environmental impact by limiting the use of potentially harmful or toxic levels of reagents. Effectively CHFS reduces the synthetic process time to a matter of seconds and is readily scalable.¹² It is controllable, producing, due to fast nucleation and growth rate,[†] a range of materials for a diverse spectrum of applications with well-defined and desirable particle properties, including size, composition, and surface area. Indeed, the recent work fosters innovative CHFS approaches in producing high quality 2D graphene (with superior antibacterial properties)⁴ adding new functionalities to the 2D substrate *via* surface functionalization with various nanostructures such as ceria-zirconia,¹³ and ceria-lanthana-zirconia¹⁴ (both exhibiting enhanced catalytic properties than graphene alone for conversion of CO₂ to value added chemicals). These examples illustrate that CHFS can deliver 2D derivatives with a high degree of control over the composition, shape and size giving significant improvement/enhancement to the aforementioned properties to those currently available.

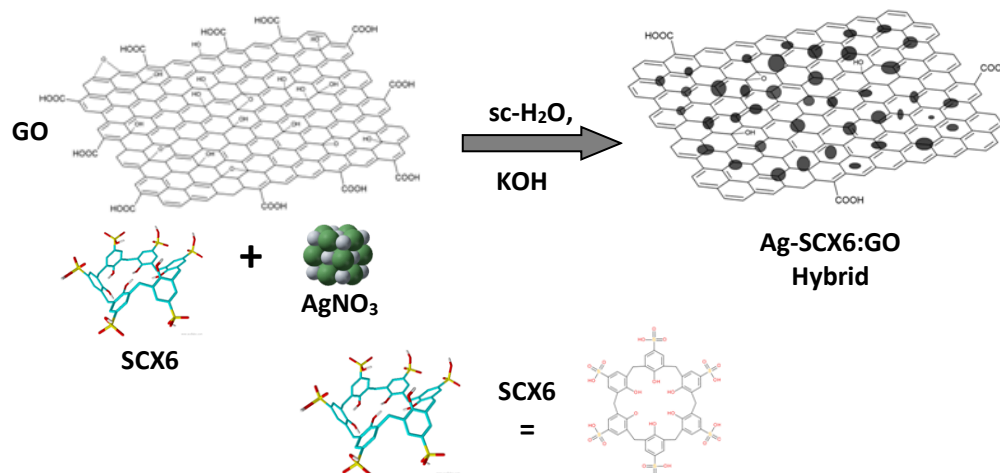
An important consideration in the production of silver nanoparticles is their instability and tendency to agglomerate, and with respect to the CHFS reactor, it is critically important to avoid blockages within the hydrothermal reaction tubing, caused by the amalgamation of liquid phase Ag during sub-critical temperatures.⁹ To overcome the agglomeration and instability of silver nanoparticles in production it is imperative to use a surfactant that stabilizes the nanoparticles. In

[†] Moreover, its exotic properties change dramatically around the critical temperature and pressure (e.g. the density of pure water varies from 0.9-0.3 g cm⁻³ and the dielectric constant varies between 2-80).

addition to this, surfactants can improve the long-term stability of Ag nanoparticles, and have also been shown to play a role in controlling the nanocrystal shape and particle size distribution.⁹

In addressing this we proposed *p*-sulphonic acid calix[6]arene (SCX6) as the surfactant stabilizer. Calixarenes in general are a class of macrocycles comprised of phenol groups linked *via* methylene bridges at the ortho position, (Scheme 1), constructed by the condensation of *p*-substituted phenols with formaldehyde.¹⁵ A variety of calixarenes derivatives have been utilized for a range of important roles in many applications; examples include the use of *p*-phosphonated calixarene as surfactant, templating agent, and stabilizer to synthesize Ag nanoparticles where the phosphonated groups improved the water solubility of the Ag nanoparticles.¹⁰ Other examples reported the ability of sulphonato-calixnaphthalene-capped silver nanoparticles for molecular recognition studies.¹⁶ Furthermore, functionalized multi-walled carbon nanotubes with calix[4]arene for use as a modified electrode to select and determine ultra-trace amounts of Pb²⁺.¹⁷ Interestingly calix[n]arene in some of its many guises have also been used as therapeutic anti-oxidant delivery systems, simultaneously displaying their own inherent anti-oxidant capability¹⁸ and slight antimicrobial behavior against bacterial and fungal species, particularly the sulfonated calixarenes.¹⁵ This allows for modification of the surface property of the silver nanoparticles (from hydrophobic to hydrophilic) and thereby broaden their potential for applications as an antibacterial agent, sensor or as catalytic materials.

Herein, we report *p*-hexasulfonic acid calix[6]arene (SCX6) assisted synthesis of pure silver and silver graphene nanocomposites *via* CHFS approach and a study of their antibacterial properties (Scheme 1,2). The products were characterized using transmission electron microscopy (TEM), powder X-ray diffraction (XRD), X-ray photoelectron spectroscopy (XPS), Raman spectroscopy and UV-Vis spectrophotometry.



Scheme 1. Schematic illustration summarizing the processing approach to synthesize Ag-rGO nanocomposites in alkaline conditions (KOH) using graphene oxide (GO) and silver nitrate (AgNO₃) assisted by *p*-hexasulphonic acid calix[6]arene (SCX6) *via* CHFS reactor.

METHODS

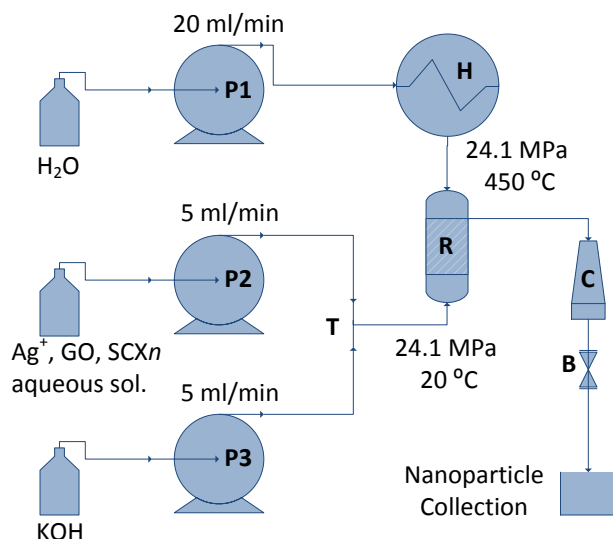
2. Experimental

2.1 Chemicals and Reagents. Silver nitrate (AgNO₃), hydrochloric acid (HCl %), sulphuric acid (H₂SO₄, 98%), natural graphite powder (NPG), sodium nitrate (NaNO₃ %), hydrogen peroxide (H₂O₂, 30%), potassium hydroxide pellets (KOH, %) and potassium permanganate (KMnO₄, 99.9%) were purchased from Fisher Scientific, UK. In all cases 10 MΩ deionized water was used. All chemicals were used without any further purification.

2.2. Synthetic processes. Graphene Oxide (GO) was synthesized using a modified Hummers method from graphite.⁴ The as-prepared GO was then used as a precursor for the synthesis of Ag-graphene nanocomposites.

p-Hexasulfonic acid calix[6]arene (SCX6) was synthesized *via* adaptation of previously reported methods.^{19a,b,c}

CHFS experiments for synthesis of Ag and Ag-graphene nanocomposites were conducted using a flow reactor designed according to that reported previously,⁴ schematic of which is shown in Scheme 2. The system employs three high performance liquid chromatography (HPLC) pumps used for the delivery of aqueous solution of reagents. Pump 1 (labelled as “P1”) was dedicated for delivering DI water through a custom made pre-heater (labelled as “H”) at a flow rate of 20 mL min⁻¹. Pump 2 (P2) and 3 (P3) were used for pumping mixtures of pre-mixed aqueous solution of precursors, for example; AgNO₃ (15 mM), SCX6 (1 mg mL⁻¹) and GO (4 μg mL⁻¹) solution (P2) and KOH (0.2 M) solution (P3) at a flow rate of 5 mL min⁻¹.



Scheme 2. Schematic of the Continuous Hydrothermal Flow Synthesis (CHFS) reactor utilized for the synthesis of Ag-rGO nanoparticles. Key: (P) HPLC pump, (T) T-junction, (H) heater, (R) reactor, (C) cooler, (BPR) back-pressure regulator.

The materials were synthesized at different compositions where the volumetric ratio of Ag^+ : GO was varied as either 1:1 or 1:2 and SCX6 concentration was constant, represented as Ag-SCX6:GO (1:1) and Ag-SCX6:GO (1:2) respectively. Pure Ag in the presence of just SCX6 was also synthesized and denoted as Ag-SCX6. In a typical experiment, AgNO_3 solution and SCX6 were added to a pre-sonicated (30 min) GO dispersion in DI water. This was pumped (*via* pump P2) to meet a flow of KOH (0.2 M delivered *via* P3) at a T-junction (T) from where the mixture then proceeded to meet superheated water (450 °C, 24.1 MPa delivered *via* P1) inside the counter-current mixer (R in Scheme 2), to give product formation in a continuous manner. The product suspension then passed through a vertical cooler (C in Scheme 2) and the slurries were collected from the exit of the back-pressure regulator (BPR in Scheme 2). The obtained products were centrifuged and freeze-dried to obtain powders for further characterization.

2.3 Characterization Techniques. *Raman Spectroscopy:* Raman spectra were collected between 50 and 3500 cm^{-1} using a confocal Labram HR300 Raman spectrometer (Horiba Jobin YvonTM) of 300 mm focal length equipped with a holographic grating of 1800 gr.mm^{-1} coupled to a Peltier cooled front illuminated CCD detector, 1024 x 256 pixels in size. Such configuration allowed for reaching a spectral resolution of about 1.4 cm^{-1} per pixel. The excitation line at 532 nm was produced by a diode-pumped solid state laser (Laser QuantumTM) focused on the sample using a MitutoyoTM 50 x long working distance objective (0.42 N.A.). Laser power at the sample was 25 mW. Spectra were corrected from a linear baseline and peak characteristics were obtained by fitting Voigt profiles to the Raman bands using the fitting software PeakfitTM.

X-ray powder diffraction and Rietveld quantitative analysis: All data were collected on a low background silicon sample holder in Bragg-Brentano geometry on a D8 Bruker diffractometer equipped with primary Gobel mirrors for parallel Cu K α X-rays and a Vantec position sensitive

linear detector. Collections conditions were: 20-120° in 2θ , 0.04 step size, 450 seconds/step, divergence slits 0.6 mm. An empirical background was collected with an empty sample holder and manually scaled and subtracted from the diffractograms. Rietveld refinements were performed with software Topas 4.1.²⁰ Spherical harmonics were used to correct for preferred orientation. A shifted Chebyshev function with eight parameters was used to fit the background. LaB₆ NIST standard was used to model the instrumental contribution to peak broadening. The sample contribution to the peak broadening was assumed to be purely Lorentzian, isotropic and purely related to size. We here remind that the e.s.d. from the Rietveld calculation has no bearing on the accuracy or otherwise of the quantification itself, being merely related to the mathematical fit of the model.²¹

Transmission Electron Microscopy (TEM): The particle size and morphology of as-prepared samples were investigated using a JEOL 2100FCs with a Schottky Field Emission Gun transmission electron microscope (200 kV accelerating voltage). Samples were collected on carbon-coated copper grids (Holey Carbon Film, 300 mesh Cu, Agar Scientific, UK) after being briefly dispersed ultrasonically in water. Particle size analysis was performed using ImageJ particle size analysis software with IBM SPSS Statistics 21. All nanocomposites re-dispersed in DI water following powder form.

X-ray photoelectron spectroscopy (XPS): XPS measurements were performed using a Kratos Axis ultra DLD photoelectron spectrometer utilizing monochromatic Alka source operating at 144 W. Samples were mounted using conductive carbon tape. Survey and narrow scans were performed at constant pass energies of 160 and 40 eV, respectively. The base pressure of the system is *ca.* 1×10^{-9} Torr, rising to *ca.* 4×10^{-9} Torr under analysis of these samples.

UV-Vis Spectrophotometry analysis: UV-Vis spectrophotometry performed using a UV-1800 Shimadzu Spectrophotometer with UV Probe software measuring the absorbance between 200-800 nm.

2.4 Evaluation of Antibacterial Activity of Ag-rGO Materials. *Determination of minimum inhibitory concentrations (MIC):* The antibacterial activity of the compounds being studied were tested using the gram negative bacterium *Escherichia coli* (ATCC 47076) and the gram positive bacterium *Staphylococcus aureus* (8325-4). To determine MIC values an overnight culture of *E. coli* or *S. aureus* was diluted into fresh LB media (10 g L⁻¹ tryptone, 5 g L⁻¹ yeast extract, 5 g L⁻¹ NaCl) to give a concentration of approximately 10⁶ cfu mL⁻¹. The culture was aseptically transferred to a microtitre plate and the compounds being tested for antimicrobial activity were added at various concentrations ranging from 1000 µg mL⁻¹ to 0.01 µg mL⁻¹. The plate was incubated overnight at 37 °C and the concentration of compound that resulted in visible inhibition of growth was determined the following day. Kanamycin and ampicillin were included as controls. Each experiment was performed in triplicate and the results shown are the mean values.

In vitro cytotoxicity by MTT [3-(4,5-dimethylthiazol)-2-diphenyltertrazolium bromide] assay: The macrophage cell line RAW 264.7 (ATCC TIB-71) was grown in fully supplemented Dulbecco's modified Eagle medium (DMEM) containing 10% fetal calf serum, 100 U mL⁻¹ penicillin and 100 µg mL⁻¹ streptomycin. Cells were seeded in 96 well tissue-culture treated microtitre plates at a density of 5 x 10⁴ cells per well and allowed to grow for 24 hours in an incubator (37°C, 5% CO₂) before the sample being tested was added. Samples were added to final concentrations ranging from 100 µg mL⁻¹ to 1.56 µg mL⁻¹. After 24 hours incubation with sample, cell viability was tested using the MTT assay. MTT dissolved in phosphate buffered saline was added to each well at a final concentration of 1 mg mL⁻¹ and the plate returned to the incubator for

3 h. The media was then aspirated and 100 μ L DMSO added to each well. The plate was shaken for *ca.* 10 minutes at room temperature and the optical density (OD) measured at 544 nm. Cell viability was reported as a percentage value compared to untreated cells and was given by the formula: cell viability (%) = $(OD_{\text{treated}} / OD_{\text{control}}) \times 100\%$, where treated cells are those that were incubated with sample being tested and control cells were incubated under the same conditions but in the absence of any sample. Each sample was assayed in triplicate and the experiment repeated twice. Results shown are the mean values and error bars represent standard deviation.

RESULTS and DISCUSSION

Herein, Ag and Ag-graphene nanocomposites were synthesized using a Continuous Hydrothermal Flow Synthesis (CHFS) route and in the presence of *p*-hexasulfonic acid calix[6]arene (SCX6) as the particle stabilizer along with aqueous KOH (0.2M) as an activator for the reduction of silver.²² The nanocomposites of Ag-graphene were made from pre-mixed Ag^+ , GO (made *via* Hummers method from graphite) and SCX6 solution, where the ratio of Ag^+ :GO was varied to 1:1 and 1:2. Additionally, pure metallic Ag was synthesized from pre-mixed aqueous solution of $AgNO_3$ and SCX6 under alkaline conditions. Samples are labelled based on their composition, e.g. Ag-SCX6 represents pure Ag synthesized in the presence of SCX6; Ag-SCX6:GO (1:1) and Ag-SCX6:GO (1:2) represents Ag-graphene nanocomposite at different ratio. All samples were synthesized in the presence of SCX6 and all other experimental conditions were kept constant ($T = 450\text{ }^\circ\text{C}$ and $P = 24.1\text{ MPa}$).

Lester and co-workers had previously reported that the formation of metallic silver *via* CHFS reactors to be problematic and was considered a consequence of the agglomeration and instability of the silver nanoparticles resulting in blockages within the hydrothermal reactor tubing, due to

amalgamation of the liquid phase Ag during sub-critical temperatures.⁹ Indeed, during our preliminary CHFS work we experienced blockages within a very short timeframe even at low concentrations of the silver precursor. Our approach to overcome this was by introducing SCX6 into the synthesis. This not only prevented the silver nanoparticles adhering to the CHFS reactor walls but also allowed the reaction chemistry to be conducted at higher precursor concentrations in addition to stabilization of nanoparticles during synthesis. The presence of KOH has been reported to be crucial to the formation of metallic silver.²² The formation mechanism of Ag nanoparticles under alkaline conditions is suggested to proceed *via* deprotonation of phenolic moieties of (i) SCX6¹⁰ and (ii) graphene oxide²² that provide sites for Ag⁺ to interact with. In particular, graphene oxide contains oxygenated functionalities such as carboxylic groups located at the edges as well as epoxide and hydroxyl groups positioned on the surface of its hexagonal basal plane, the latter becoming a phenolic entity.² The phenol groups which are present in both SCX6 and graphene oxide are known to undergo deprotonation^{10,22} under basic conditions to produce strongly activated phenolate anions, which proceed *via* electrophilic substitution by transferring electrons to the Ag⁺ ions to produce metallic silver.²²

Transmission Electron Microscopy (TEM) (Figure 1) was employed to study the morphology and to determine the particle size of all compositions. Moreover, to give further insight into structural information of the metallic Ag nanoparticles, HRTEM images are also included as well as the corresponding selected-area electron diffraction patterns. These images revealed that Ag particles are of spherical morphology consisting of well-ordered single crystals with lattice fringes corresponding to crystalline metallic silver.²² The measured fringe spacing of the lattice planes were determined to be 0.26 ± 0.02 nm for sample Ag-SCX6 (Figure 1b). These values correspond to d-spacing [111] for face-centered cubic (fcc) Ag.²²

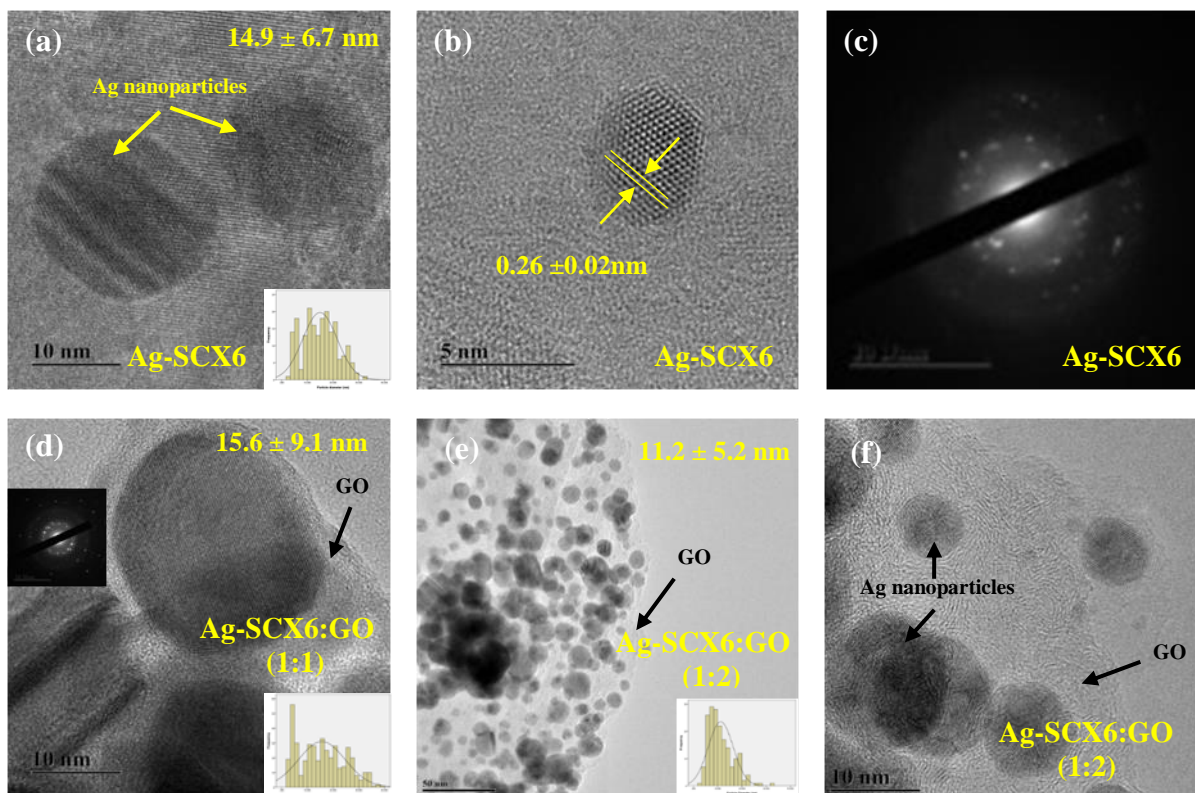


Figure 1: Morphological and particle sizing studies of nanocomposites; Transmission Electron Microscopy (TEM) images of metallic Ag nanoparticles, the corresponding selected-area electron diffraction and Ag-graphene nanocomposites with representative particle size vs. frequency graph (inserts).

The selected area electron diffraction (SAED) feature also confirms the metallic crystalline nature of silver. The TEM images of Ag-graphene nanocomposites clearly demonstrated that the rGO sheets are uniformly decorated with Ag nanoparticles. Interestingly, Ag nanoparticles were noted to be easily susceptible to electron beam-induced aggregation, a phenomena which has been reported previously, thus the presence of larger Ag nanoparticles observed is due to the agglomeration of smaller particles.²³

The crystallinity and phase composition of the pure silver and silver-graphene nanocomposites was assessed by X-ray powder diffraction (XRD) where their diffraction patterns are shown in Figure 2 (refinement plots in ESI). The observed diffraction peaks were indexed to the [111], [200], [220], [311] and [222] planes of face-centered-cubic metallic Ag.⁸

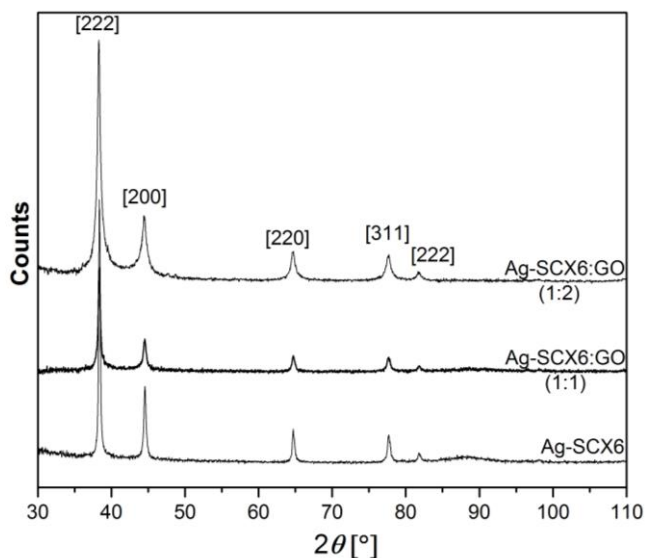


Figure 2. XRD patterns for Ag and Ag-Graphene nanocomposites

No diffraction peaks assigned to silver oxide or any metal salt precursors were observed, which indicates the purity and high quality of metallic silver synthesized *via* CHFS. Notably, in the XRD patterns of Ag-graphene nanocomposites, the characteristic peak (002) of graphitized material typically located at $2\theta = 25.32^\circ$ is not observed.⁴ This can be explained by the fact that phases with heavy elements diffract X-rays far more intensely than those with light elements as well as a small amount of material (1-2 mg) was used for the XRD analysis. However, the presence of graphene is confirmed *via* other techniques such as TEM, XPS and Raman. Furthermore, the Debye–Scherrer formula was applied to the XRD data assuming a pure Lorentzian sample contribution to the peak broadening to determine and compare the crystallite sizes in all compositions (Table 1).

The pure Ag sample synthesized in the presence of SCX6 (sample labelled as Ag-SCX6) exhibited the largest crystallite size of 5.5 ± 0.1 nm. Contrastingly, the Ag component of the Ag-SCX6:GO (1:2) nanocomposite had the smallest crystallite size of 1.42 ± 0.02 nm, whereas the Ag-SCX6:GO (1:1) exhibited an intermediate value.

Table 1 Lattice parameter for all samples with relative e.s.d. (in parenthesis), crystal size and χ^2 as obtained from the Rietveld refinements.

Sample ID	a (Å)	Crystal size (nm)	χ^2
Ag-SCX6	4.08521 (± 0.00035)	5.5 (± 0.1)	2.45
Ag-SCX6:GO (1:1)	4.08481 (± 0.00066)	2.94 (± 0.08)	2.18
Ag-SCX6:GO (1:2)	4.08638 (± 0.00067)	1.42 (± 0.02)	2.45

For analysis of the changes in the chemical states of the as-prepared Ag and Ag-graphene nanocomposite materials, X-ray photoelectron spectroscopy (XPS) was utilized, the spectra of which are shown in Figure 3. As we have previously reported,²⁵ the CHFS route is efficient in dehydrating/reducing graphene oxide. Indeed, the deconvoluted C(1s) XPS spectra (Figure 3a) of materials made hydrothermally revealed significant reduction of peak intensities of the oxygen containing functional groups (epoxide, carboxyl and hydroxyl) which are associated with GO (starting material). Furthermore, the XPS spectra reveal significant amount of carbon for the pure Ag samples which we assign to the presence of the calixarene and supported by a S(2p) energy of 168.1 eV, characteristic of sulfur-oxygen bonds, such as those present in calixarene. The Ag(3d_{5/2}) binding energy was found to be at 368.3 eV (Figure 3b) together with small loss features to the higher binding energy side of the main photoelectron peak indicative of metallic Ag. Analysis of

the x-ray induced Auger peaks (figure 3c) also revealed a spectral shape and modified Auger parameter of *ca.* 726 eV again consistent with metallic Ag

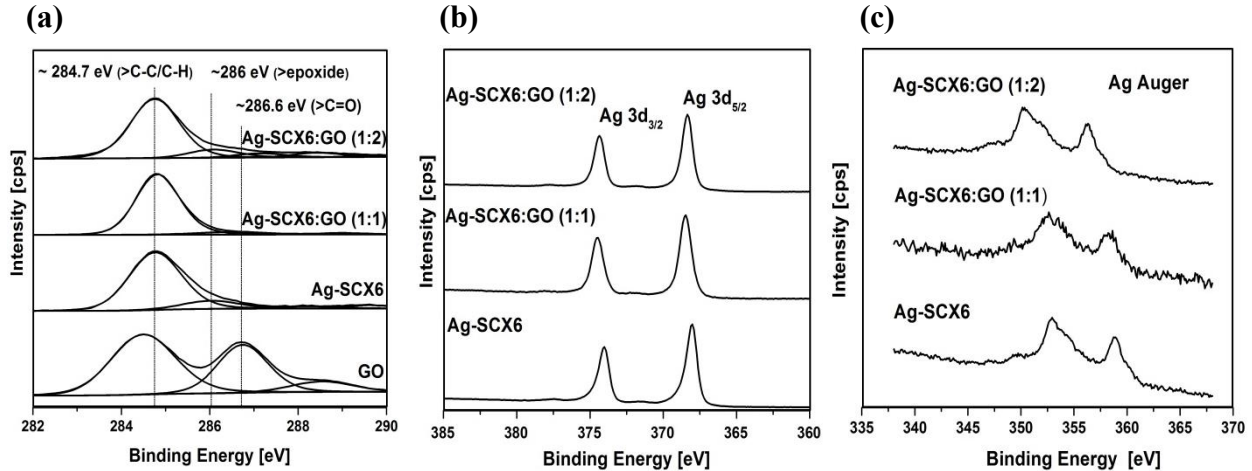


Figure 3: XPS spectra of C1 s (a), core level Ag 3d (b), and Ag Auger (c) for Ag-SCX6 and Ag-SCX6:rGO nanocomposites.

By using Raman spectroscopy, the chemical microstructure and functionalization of graphene sheets with silver could be characterized further. The Raman spectrum of graphene oxide presented two characteristic broad Raman bands around $\sim 1357 \text{ cm}^{-1}$ and 1586 cm^{-1} ,²⁴ corresponding to the D and G bands respectively, and are present in all poly-aromatic hydrocarbons.²⁵ The D Raman band is due to the A_{1g} breathing modes of six-atom rings and requires a defect for its activation whereas the G band corresponds to the tangential stretching mode of the E_{2g} phonon of an sp^2 carbon atom²⁶ and is not affected by the presence of defects. The intensity ratio of these two bands (I_D/I_G) provides information on the degree of disorder and the average size of the sp^2 domains. Raman spectra of silver and silver graphene composites (Ag-SCX6:GO) are presented in Figure 4. A significant increase of the full width at half maximum (FWHM) is observed for both the D and G bands for Ag-SCX6:GO. This increase of FWHM indicates a decrease of crystallinity and

a progressive amorphization of the graphene layers in the Ag-GO samples. In addition, the ratio of intensity of the D band to that of the G band (I_D/I_G) also increases from GO (0.95) to 1.07 and 1.09 for Ag-GO samples. This ratio increase is consistent with the literature and is assigned to the reduction of graphitic domains, resulting from functionalization of GO sheets with silver nanoparticles.²⁷ Frequently, pure silver is employed for Surface Enhanced Raman Scattering (SERS) a technique used to enhance the Raman signal of various molecules. Vibrational bands corresponding to silver were observed at 989 cm^{-1} , 1078 cm^{-1} , 1350 and 1574 cm^{-1} , confirming the presence of Ag on the graphene.²⁷

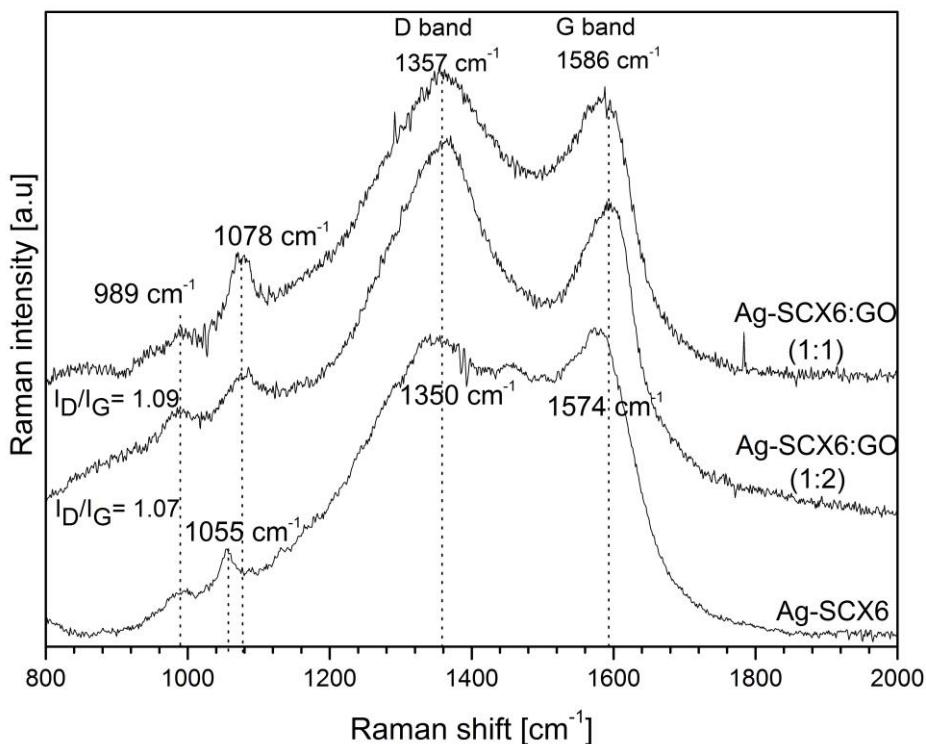


Figure 4: Raman spectra for Ag and Ag-Graphene nanocomposites

The spectrum from the UV-Vis spectrophotometry analysis (Figure 5) indicates the presence of silver nanoparticle formation for the three nanocomposites samples (Ag-SCX6, Ag-SCX6:GO

(1:1), and Ag-SCX6:GO (1:2)) with an absorption peak at approximately 421, 412, and 407 nm, respectively, assigned to the excitation of surface plasmon for Ag nanoparticles.²² The two Ag-graphene composites however, display a somewhat continued absorbance peak from *ca.* 450 nm. This is believed to occur due to two possible factors: (1) the presence of graphene lowering the absorbance of the Ag particles, which fits that the Ag-SCX6-graphene composites, with increasing GO ratio, display less defined peaks compared to the standalone Ag-SCX6 sample, (Figure 5), and, (2) as has previously been described,²² when silver-graphene powders are re-dispersed in water, the UV-Vis absorption spectrum shows a characteristic continued absorbance from 400-800 nm, making it difficult to define the Ag nanoparticle peak from approximately 410 nm onwards. UV-vis spectrum of SCX6 revealed π - π^* transitions centred at *ca.* 276 and 283 nm. It may also be plausible to confer from the spectra of calixarene (SCX6 dotted line Figure 5) from the apparent should peaks being observed from approximately 276 nm in each of the Ag-SCX6 samples. However, as expected there is no SCX6 corresponding peak observed for the rGO sample alone.

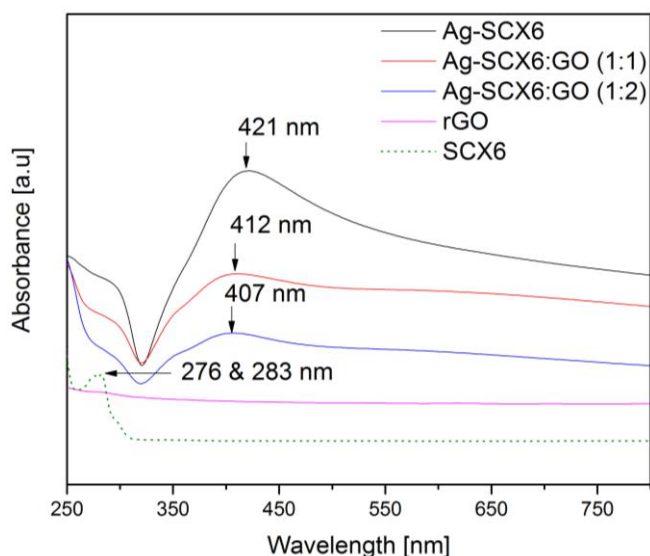


Figure 5. UV-Vis absorption spectrum for all Ag-nanocomposites, reduced graphene oxide, and sulfonic acid calix[6]arene.

Antibacterial Activity. The minimum inhibitory concentration (MIC) of each compound was determined against either a gram negative (*Escherichia coli* MG1655) or gram positive (*Staphylococcus aureus* 8325-4) bacterium as described in material and methods.

The results from the MIC assays suggest that the combination of Ag with GO dramatically improves the antimicrobial activity of standalone Ag while simultaneously reducing the concentrations required in exerting the desired effect against both bacterial strains. The pure Ag-SCX6 sample shows the highest MIC value at $5.6 \mu\text{g mL}^{-1}$, therefore the lowest antibacterial activity of all the Ag-containing compounds tested against *S. aureus* (Table 2). Against *E. coli* the same sample material, Ag-SCX6, displayed an improved antibacterial performance over both reference antibiotics with a MIC value of $2.5 \mu\text{g mL}^{-1}$, however, this paled in comparison to the silver-graphene nanocomposites, Ag-SCX6:GO (1:1) and Ag-SCX6:GO (1:2), which gave MIC values of 0.7 and $0.35 \mu\text{g mL}^{-1}$ respectively,(Table 2).

Table 2. The minimum inhibitory concentrations (MIC) of each sample, and the reference antibiotics, determined against *Staphylococcus aureus* (8325-4) and *Escherichia coli* (MG1655).

Compound	<i>S. aureus</i>	<i>E. coli</i>
	MIC ($\mu\text{g mL}^{-1}$)	MIC ($\mu\text{g mL}^{-1}$)
Ag-SCX6	5.6	2.5
Ag-SCX6:GO (1:1)	2.5	0.7
Ag-SCX6:GO (1:2)	1.4	0.35
Kanamycin	2.8	5.6
Ampicillin	0.1	5.6

Interestingly, the addition of GO considerably lowers the MIC value for all Ag calixarene:GO variants against both bacteria strains, thus further improving the compound's antibacterial activity. This is especially true for the compounds with a higher ratio of GO to Ag, Ag-SCX6:GO 1:2. For *E. coli* both Ag-GO nano-composites show greater antibacterial activity over kanamycin or ampicillin alone, with the lowest MIC values of $0.35 \mu\text{g mL}^{-1}$ being determined for the Ag-SCX6:GO (1:2) sample (Table 2), whilst against *S. aureus* the addition of Ag-SCX6:GO (1:2) results in a MIC of $1.4 \mu\text{g mL}^{-1}$, which is lower than kanamycin, but not as effective against ampicillin (Table 2).

The toxicity of each of the compounds was determined against the murine macrophage cell line Raw264.7 using an MTT assay as described in materials and methods. The data (Figure 6) shows that at relatively high concentrations ($100 \mu\text{g mL}^{-1}$) all compounds result in varying degrees of cell death (>80% for Ag-SCX6:GO (1:2) to approximately 55% for Ag-SCX6).

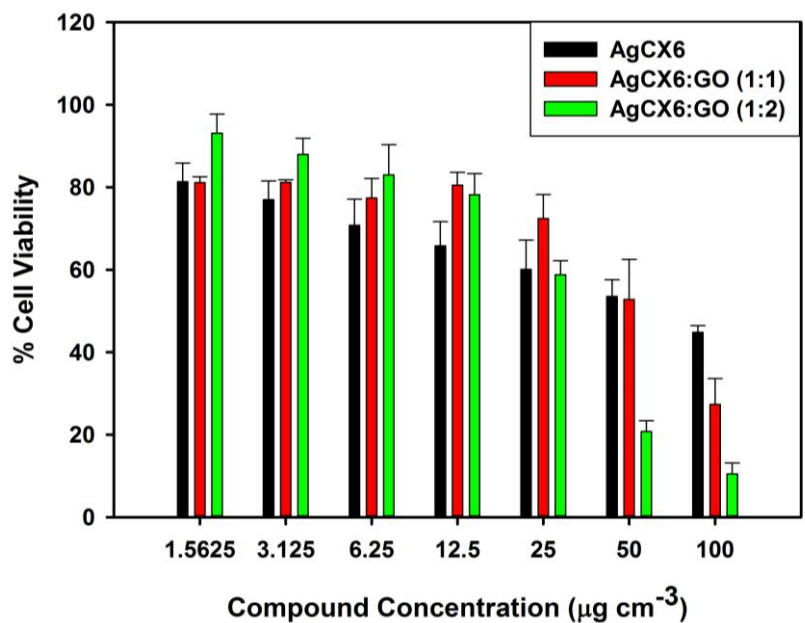


Figure 6. Viability of RAW 264.7 cells after incubation with silver-graphene nanocomposites at varying concentrations for 24 hours.

However, as the concentration of each compound decreases, so does the amount of cell death. Whilst Ag-SCX6:GO (1:2) displays the greatest toxicity at $100 \mu\text{g mL}^{-1}$, it also displays negligible toxicity at concentrations less than $12.5 \mu\text{g mL}^{-1}$, and as the MICs against either *S. aureus* or *E. coli* are approximately 10 and 35 times lower (respectively) than this value, it suggests that these compounds may merit further study as potential antibacterial compounds with relatively low toxicity to eukaryotic cells.

The antimicrobial activity and mechanisms of action for both Ag and graphene have been examined previously,^{4,28} however, more is required to fully elucidate the process when these materials are combined. Ag nanoparticles have demonstrated the ability to disrupt the cell membranes of gram negative *E. coli*^{28c} and strongly inhibit the cell division of gram positive *S. aureus*,^{1,28c} via negative interaction with the microbial cell membrane. Graphene nanosheets have

been shown to have standalone antimicrobial activity.⁴ This is thought to be due to the destruction of bacterial cell membrane integrity through physical contact by sharp nanosheets, and possibly oxidative damage via the formation of reactive oxygen species (ROS).^{4, 5, 28b} Alone however, these antibacterial activities have not been shown effective enough to compete with known commercial antibiotics.

The combination of Ag and rGO in the form of a composite nanomaterial, or hybrid, has clearly improved the antibacterial activity of the two materials, which may be enhanced through the graphene nanosheets ability to; (1) provide a negatively charged surface for the Ag nanoparticle to be deposited on, resulting in minimal agglomeration of the Ag nanoparticles, which has been shown to improve their antimicrobial effect,^{8, 29} and/or (2) to adhere to the bacteria cell walls and thus, acting as a delivery system, increase the chance of proximity interactions between the Ag and the microbes, and/or (3) the rGO sheets increase the potency of the antibacterial properties through composite synergistic effect. The strategy, whereby the graphene sheets wrap the bacterial cells and act synergistically with the Ag nanoparticles to execute a potent antimicrobial effect, has been described as a ‘capturing-killing process’.⁸

CONCLUSIONS

To conclude, we have developed a new approach toward synthesis of highly functional hybrid nano-materials, which combines the individual precursor properties to produce an enhanced antibiotic activity effect against both gram positive and negative bacteria. Using the CHFS process enabled a continuous, rapid, highly tailored production of said materials, while minimizing the use of potentially hazardous chemicals normally involved in their synthesis. The assistance of multifunctional *p*-sulfonic acid calix[6]arene in both the prevention of Ag particle blockages of

the CHFS reactor tubing, and the formation and stability of Ag nanoparticles deposited on graphene sheets, not only allowed the synthesis to be successful through the reactor but provided another possible point of control for particle size and distribution. Furthermore, the preliminary findings which show possible improvements in antibiotic activity for our Ag-graphene hybrids over the reference antibiotics, ampicillin and kanamycin, provide a new avenue of investigation towards battling the ever increasing antibacterial resistance developing in pathogenic microbes.

ASSOCIATED CONTENT

Supporting Information.

XRD refinement plots. This material is available free of charge via the Internet at <http://pubs.acs.org>.”

AUTHOR INFORMATION

Corresponding Author

*Email: kellicis@lsbu.ac.uk

Author Contributions

The manuscript was written through contributions of all authors. All authors have given approval to the final version of the manuscript.

Funding Sources

The financial support was provided by London South Bank University.

ACKNOWLEDGMENT

S. Kellici, A. Vaughn, N. P. Power and J. Acord gratefully acknowledge the financial support provided by LSBU. We acknowledge Mr. Steve Jones (LSBU) for his technical support with the development of CHFS reactor.

ABBREVIATIONS

CHFS - Continuous Hydrothermal Flow Synthesis (CHFS); SCX6 - *p*-hexasulfonic acid calix[6]arene; TEM - transmission electron microscopy; XPS - X-ray photoelectron spectroscopy, XRD - X-ray powder diffraction; MIC - minimum inhibitory concentration; FWHM - full width at half maximum; *E. coli* - Escherichia coli (Gram negative) bacteria; *S. aureus* - Staphylococcus aureus (Gram-positive bacteria)

REFERENCES

- (1) Franci, G.; Falanga, A.; Galdiero, S.; Palomba, L.; Rai, M.; Morelli, G.; Galdiero, M. Silver Nanoparticles as Potential Antibacterial Agents. *Molecules* **2015**, *20* (5), 8856–8874
- (2) (a) Gao, P.; Nie, X.; Zou, M.; Shi, Y.; Cheng, G. Recent Advances in Materials for Extended-Release Antibiotic Delivery System. *J. Antibiot. (Tokyo)*. **2011**, *64* (9), 625–634. (b) McGowan, J. E. Economic Impact of Antimicrobial Resistance. *Emerg. Infect. Dis.* **2001**, *7* (2), 286–292.
- (3) Liu, Y.; He, L.; Mustapha, A.; Li, H.; Hu, Z. Q.; Lin, M. Antibacterial Activities of Zinc Oxide Nanoparticles against Escherichia Coli O157:H7. *J. Appl. Microbiol.* **2009**, *107* (4), 1193–1201.

- (4) Kellici, S.; Acord, J.; Ball, J.; Reehal, H. S.; Morgan, D.; Saha, B. A Single Rapid Route for the Synthesis of Reduced Graphene Oxide with Antibacterial Activities. *RSC Adv.* **2014**, *4* (29), 14858.
- (5) Hu, W.; Peng, C.; Luo, W.; Lv, M.; Li, X.; Li, D.; Huang, Q.; Fan, C. Graphene-Based Antibacterial Paper. *ACS Nano* **2010**, *4* (7), 4317–4323.
- (6) Marciano, F. R.; Lima-Oliveira, D. A.; Da-Silva, N. S.; Diniz, A. V.; Corat, E. J.; Trava-Airoldi, V. J. Antibacterial Activity of DLC Films Containing TiO₂ Nanoparticles. *J. Colloid Interface Sci.* **2009**, *340* (1), 87–92.
- (7) Rajan, A.; Vilas, V.; Philip, D. Studies on Catalytic, Antioxidant, Antibacterial and Anticancer Activities of Biogenic Gold Nanoparticles. *J. Mol. Liq.* **2015**, *212*, 331–339.
- (8) Xu, W.-P.; Zhang, L.-C.; Li, J.-P.; Lu, Y.; Li, H.-H.; Ma, Y.-N.; Wang, W.-D.; Yu, S.-H. Facile Synthesis of Silver@graphene Oxide Nanocomposites and Their Enhanced Antibacterial Properties. *J. Mater. Chem.* **2011**, *21* (12), 4593-4597.
- (9) Aksomaityte, G.; Poliakoff, M.; Lester, E. The Production and Formulation of Silver Nanoparticles Using Continuous Hydrothermal Synthesis. *Chem. Eng. Sci.* **2013**, *85*, 2–10.
- (10) Hartlieb, K. J.; Saunders, M.; Raston, C. L. Templating Silver Nanoparticle Growth Using Phosphonated Calixarenes. *Chem. Commun.* **2009**, 3074–3076.
- (11) Zangeneh Kamali, K.; Pandikumar, A.; Sivaraman, G.; Lim, H. N.; Wren, S. P.; Sun, T.; Huang, N. M. Silver@graphene Oxide Nanocomposite-Based Optical Sensor Platform for Biomolecules. *RSC Adv.* **2015**, *5* (23), 17809–17816.

- (12) Tighe, C.J.; Cabrera, R.Q.; Gruar, R.I.; Darr, J.A. Scale Up Production of Nanoparticles: Continuous Supercritical Water Synthesis of Ce-Zn Oxides. *Ind. Eng. Chem. Res.* **2013**, *52* (16), 5522-5528.
- (13) Saada, R.; Kellici, S.; Heil, T.; Morgan, D.; Saha, B. Greener Synthesis of Dimethyl Carbonate Using a Novel Ceria–zirconia Oxide/graphene Nanocomposite Catalyst. *Appl. Catal. B Environ.* **2015**, *168-169*, 353–362.
- (14) Adeleye, A. I.; Kellici, S.; Heil, T.; Morgan, D.; Vickers, M.; Saha, B. Greener Synthesis of Propylene Carbonate Using Graphene-Inorganic Nanocomposite Catalysts. *Catal. Today* **2015**, *256*, 347–357.
- (15) Lamartine, R.; Tsukada, M.; Wilson, D.; Shirata, A. Antimicrobial Activity of Calixarenes. *Comptes Rendus Chim.* **2002**, *5* (3), 163–169.
- (16) Valluru, G.; Georghiou, P. E.; Sleem, H. F.; Perret, F.; Montasser, I.; Grandvoinet, A.; Brolles, L.; Coleman, A. W. Molecular Recognition of Nucleobases and Amino Acids by Sulphonato-Calixnaphthalene-Capped Silver Nanoparticles. *Supramol. Chem.* **2014**, *26* (7-8), 561–568.
- (17) Wang, L.; Wang, X.; Shi, G.; Peng, C.; Ding, Y. Thiocalixarene Covalently Functionalized Multiwalled Carbon Nanotubes as Chemically Modified Electrode Material for Detection of Ultratrace Pb²⁺ Ions. *Anal. Chem.* **2012**, *84*, 10560–10567.
- (18) Stephens, E. K.; Tauran, Y.; Coleman, A. W.; Fitzgerald, M. Structural Requirements for Anti-Oxidant Activity of Calix[n]arenes and Their Associated Anti-Bacterial Activity. *Chem. Commun.* **2015**, *51* (5), 851–854.

- (19) (a) Gutsche, C.D.; Dhawan, B.; Leonis, M.; Stewart, D.; p-tert-butylcalix[6]arene. *Org. Synth.*, **1990**, 68, 238. (b) Lamartine, R.; Regnouf de Vains, J. B.; Choquard P.; Marcillac, A. Process for the dealkylating sulfonation of p-alkyl calixarenes. *US Patent 5952526*, **1999**. (c) Shinkai, S.; Araki, K.; Tsubaki, T.; Manabe, A. New syntheses of calixarene-p-sulphonates and p-nitrocalixarenes. *J. Chem. Soc. Perkin Trans. 1*, **1987**, 1, 2297-2299.
- (20) Vieira Coelho, A. C.; Souza Santos, H. De; Kiyohara, P. K.; Marcos, K. N. P.; Souza Santos, P. De. Surface Area, Crystal Morphology and Characterization of Transition Alumina Powders from a New Gibbsite Precursor. *Mater. Res.* **2007**, 10 (2), 183–189.
- (21) Scarlett, N. V. Y.; Madsen, I. C. Quantification of Phases with Partial or No Known Crystal Structures. *Powder Diffr.* **2006**, 21 (04), 278–284.
- (22) Pasricha, R.; Gupta, S.; Srivastava, A. K. A Facile and Novel Synthesis of Ag-Graphene-Based Nanocomposites. *Small* **2009**, 5 (20), 2253–2259.
- (23) Chandrasekar, A.; Pradeep, T. Luminescent Silver Clusters with Covalent Functionalization of Graphene. *J. Phys. Chem. C* **2012**, 116 (26), 14057–14061.
- (24) Kudin, K.N.; Ozbas, B.; Schniepp, H.C.; Prud'homme, R.K.; Aksay, I.A; Car, R. Raman Spectra of Graphite Oxide and Functionalised Graphene Sheets. *Nano Let.* **2008**, 8(1), 36-41
- (25) Ferrari, A. C. Raman Spectroscopy of Graphene and Graphite: Disorder, Electron-Phonon Coupling, Doping and Nonadiabatic Effects. *Solid State Commun.* **2007**, 143 (1-2), 47–57.
- (26) Ferrari, A. C.; Robertson, J.; Interpretation of Raman spectra of disordered and amorphous carbon. *Phys. Rev. B* **2010**, 61(20), 14095-14107.

(27) Naja, G.; Bouvrette, P.; Hrapovic, S.; Luong, J. H. T. Raman-Based Detection of Bacteria Using Silver Nanoparticles Conjugated with Antibodies. *Analyst* **2007**, *132* (7), 679–686.

(28) (a) Yamanaka, M.; Hara, K.; Kudo, J. Bactericidal Actions of a Silver Ion Solution on Escherichia Coli, Studied by Energy-Filtering Transmission Electron Microscopy and Proteomic Analysis Bactericidal Actions of a Silver Ion Solution on Escherichia Coli. *Appl. Environ. Microbiol.* **2005**, *71* (11), 7589–7593. (b) Liu, S.; Zeng, T. H.; Hofmann, M.; Burcombe, E.; Wei, J.; Jiang, R. Antibacterial Activity of Graphite, Graphite Oxide, Graphene Oxide, and Reduced Graphene Oxide: Membrane and Oxidative Stress. *ACS Nano*. **2011**, *9*, 6971–6980. (c) Tang, J.; Chen, Q.; Xu, L.; Zhang, S.; Feng, L.; Cheng, L.; Xu, H.; Liu, Z. Graphene Oxide – Silver Nanocomposite As a Highly Effective Antibacterial Agent with Species-Specific Mechanisms. *ACS Appl. Mater. Interfaces*. **2013**, *5* (9), 3867-3874.

(29) Barua, S.; Thakur, S.; Aidew, L.; Buragohain, A. K.; Chattopadhyay, P.; Karak, N. One Step Preparation of a Biocompatible, Antimicrobial Reduced Graphene Oxide–silver Nanohybrid as a Topical Antimicrobial Agent. *RSC Adv.* **2014**, *4* (19), 9777-9783.

Table of Contents Graphic and Synopsis

Demonstrated herein is a single rapid approach employed for synthesis of Ag-graphene nanocomposites, with excellent antibacterial properties and low cytotoxicity, by utilizing a Continuous Hydrothermal Flow Synthesis (CHFS) process in combination with *p*-hexasulfonic acid calix[6]arene (SCX6) as an effective particle stabilizer. The nanocomposites showed high activity against *E. coli* (Gram-negative) and *S. aureus* (Gram-positive) bacteria. The Ag-graphene nanocomposites were characterized using a range of techniques including transmission electron microscopy (TEM), X-ray photoelectron spectroscopy (XPS), Raman, and X-ray powder diffraction (XRD). This rapid, single step synthetic approach not only provides a facile means of enabling and controlling graphene reduction (under alkaline conditions), but also offers an optimal route for homogeneously producing and depositing highly crystalline Ag nanostructures into reduced graphene oxide substrate.

